Iranian Journal of Science and Technology, Transactions of Civil Engineering (2024) 48:1313–1327
https://doi.org/10.1007/s40996-024-01394-w

RESEARCH PAPER

A Comprehensive Study on the Selection of Mother Wavelets and Mode Shapes for Multiple Damage Identification

Hashem Jahangir[1] · Hamed Hasani[2] · José Viriato Araújo dos Santos[3] · Hernâni Miguel Lopes[4]

Received: 14 June 2022 / Accepted: 20 February 2024 / Published online: 15 March 2024

Abstract
The aim of this paper is to find the proper families and mother wavelets for a successful localization of multiple damages in beams. The post-processing of differences in modal rotations, experimentally measured with shearography, and differences in modal curvatures of aluminium beams are carried out with 14 wavelet families and 84 mother wavelets. The damage identifications show that the best families of wavelets for the post-processing of modal data are the Shannon, frequency B-spline, and complex Morlet families. In order to select the modes that are more sensitive to damage, a novel parameter for the evaluation of the most changed mode is proposed. The boundary effect, which is often found in wavelet-based damage identifications, is also addressed in this paper. The results show that the post-processing of differences in modal curvatures yields better damage identifications than the post-processing of differences in modal rotations.

Keywords Mother wavelets · Modal rotations/curvatures · Shearography · Beam · Multiple damage

1 Introduction

Finding initial cracks and other kinds of incipient damage in structures is the main issue of various industrial applications. As structural damage detection requirements become increasingly strict and rigorous, monitoring or testing of operational structures must be done regularly. In such inspections, non-destructive testing (NDT) is usually carried out. Therefore, these approaches aim to be sensitive to different kinds of structural damage, assess the locations and severities of such losses as early as possible to prevent collapses of structural performance, and plan maintenance operations in advance (Zhu et al. 2011). In recent years, numerous NDT techniques have been developed and further refined to meet the requirements of the current maintenance philosophies (Abdel-Latif 2009; Grandt 2011). Among the variety of non-destructive tests available today, optical methods provide non-destructive, contactless, and structural examination with a relatively high degree of sensitivity to both exterior and interior damage. Shearography is one of the most prominent methods, exhibiting high sensitivity levels thanks to its interferometric NDT technology (Abdel-Latif 2009; Grandt 2011; Lopes et al. 2012). In part, this method has a high level of sensitivity because it does not require any contact. Furthermore, unlike contact measurement systems, this type of method significantly reduces the time and cost of data acquisition (Feng and Feng 2018). Shearography allows the detection of defects and faults in a structure by direct measurement of the gradient of the modal displacement field. Although shearography was developed at the beginning of the 1970s (dos Santos and Lopes 2018), its advantages still make it an effective non-destructive testing method. In addition, shearography is recommended and approved for inspection of aircraft structures by the European Aviation Safety Agency (EASA) and has also been

✉ Hashem Jahangir
h.jahangir@birjand.ac.ir

Hamed Hasani
hamed.hasani@unipr.it

José Viriato Araújo dos Santos
viriato@tecnico.ulisboa.pt

Hernâni Miguel Lopes
hml@isep.ipp.pt

[1] Department of Civil Engineering, University of Birjand, Birjand, Iran

[2] Department of Engineering and Architecture, University of Parma, 43121 Parma, Italy

[3] IDMEC, Instituto Superior Técnico, Universidade de Lisboa, Lisbon, Portugal

[4] Department of Mechanical Engineering, DEM-ISEP, Instituto Politécnico do Porto, Porto, Portugal

recommended for use by the Federal Aviation Administration (FAA) (Katunin et al. 2021).

Due to the ability to measure structural response in a field environment without contact requirements, the NDT shearographic approach has also been found helpful in the construction industry for the inspection and identification of cracks and delaminations in concrete and steel structures (Bagheri et al. 2019; Jahangir and Esfahani 2020a, b; Jahangir et al. 2021a). Signal processing techniques (Jahangir et al. 2021b) improve the sensitivity of shearography (Zhao et al. 2018) to various forms of structural damage, which is one of the subjects of numerous research studies conducted by the authors. Prior research studies have focused on measuring differences in modal rotation using shearography (Reis Lopes et al. 2011; Lopes et al. 2014) and applying optimal spatial sampling to these measurements (Mininni et al. 2016; Katunin et al. 2018), which increased the sensitivity of the proposed approaches to structural damage. Several case studies in the authors' research focus on transforming algorithms on wavelets (Araujo Dos Santos et al. 2019; Katunin et al. 2019; Yazdanpanah et al. 2021) that helped to identify in some cases the boundaries of damaged areas. The results of previous studies show that the sensitivity and accuracy of the proposed damage indicator are highly dependent on the selected wavelet family and mother wavelets (Jahangir and Esfahani 2012, 2013; Katunin and Holewik 2013; Seyedi et al. 2015; Yazdanpanah et al. 2020), so it is crucial to make the right choice.

The continuous wavelet transform (CWT) gives a time–frequency representation of a signal. It relies on wavelet basis functions, also known as mother wavelets, that can be chosen based on satisfying the admissibility condition. Any mother wavelet is continuous in both time and frequency domains and is the source of construction of other basis functions. Several research studies have confirmed the effectiveness of CWTs in 1D and 2D damage detection in beams (Gentile and Messina 2003; Douka et al. 2003; Loutridis et al. 2004; Rucka and Wilde 2006), trusses (Mousavi et al. 2021) and plates (Douka et al. 2004; Rucka and Wilde 2006; Huang et al. 2009; Fan and Qiao 2009; Janeliukstis et al. 2017; Yang and Oyadiji 2017; Zhou et al. 2018), respectively. CWTs have been successfully applied in all these studies, regardless of their potential lack of baseline information. It is possible to further improve the detectability of structural damage through a suitable baseline, which may include experimental or numerical data acquisition in an undamaged state, as noted by Solís et al. (2013, 2018). Additionally, Solís et al. (2013, 2018) found a reduction of the boundary effect and reduced importance of noise in the post-processing of baseline and damaged data with wavelets since they are highly sensitive to disturbances (Abdulkareem et al. 2019). The boundary effect reduction was also observed by dos Santos et al. (2021) in the damage identification with differences in modal rotations.

2 Research Significance

Most previous studies in the damage detection field utilized sensors connected to the surface of the structural element to measure the vibration of responses. In this case, any small surface crack at the location of the sensors caused their detachment and stopped the measuring process. To solve this problem, non-contact sensing approaches such as shearography are beneficial, which is the core and novelty of the current study.

In this study, systematic investigations were conducted to detect multiple structural damages in aluminium beams using new methods applied to differences in modal rotations after a 1D CWT is applied. Modal rotations of one undamaged beam and two damaged beams were measured with shearography. As opposed to some previous studies conducted on the detection of damage, including a large reduction in thickness (Rucka and Wilde 2006), smaller damage cases were investigated in the present study. Indeed, one of the aluminium beams experimentally examined has an area with a thickness reduction of 7%. Additionally, the beams have multiple damage scenarios, which are still a challenge to identify because such cases are prone to false positive indications of damage locations (Nayyar et al. 2021). Although in the literature, more wavelets, which were applied to a similar class of problems, can be found, all the available wavelet families in Matlab software are selected to be evaluated in the current study. In this paper, a novel statistical method as a new metric is utilized to select the best wavelet family and related mother wavelet based on the frequency of the number of times the selected mother wavelet can detect the exact location of the damage scenarios as slots. Moreover, a damage threshold was defined based on the wavelet coefficient values to identify the damage locations by ignoring the possible noises induced in the process stage. The measured data and post-processing algorithm clearly demonstrate the effectiveness of shearography and the application of wavelet transform for damage identification. This effectiveness is also a result of the proposed selection of modal rotations that should be post-processed.

It should be mentioned that any mother wavelet has individual geometrical configurations and characteristics, which can be changed by changing the scale value. On the other hand, any damage scenario in a structural element causes a specific change in the inherent features of the structure, such as its natural frequency and mode shape. Therefore, no helpful suggestion can be provided for the users to select the

Table 1 Location, depth, width, and thickness reduction of slot 1 (S1) and slot 2 (S2)

Beam	S1				S2			
	Location [mm]	Depth [mm]	Width [mm]	Thickness reduction [%]	Location [mm]	Depth [mm]	Width [mm]	Thickness reduction [%]
B2	200	0.2	10	7	64.5	0.2	10	7
B3	200	0.85	10	28	64.5	0.85	10	28

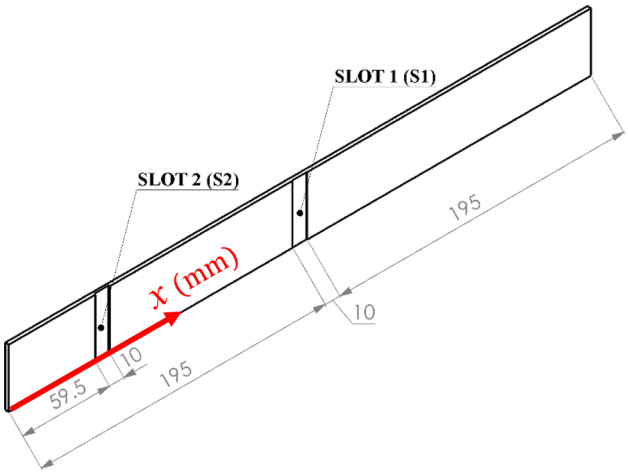

Fig. 1 Location and width of slot 1 (S1) and slot 2 (S2)

best mother wavelets before conducting the trial and error process.

3 Material and Methods

This section presents the characteristics of the beams and their damage. The shearography system used to measure the modal rotations is also described. The influence of damage is measured by parameters to evaluate the changes in natural frequencies and modes. Finally, two damage indicators based on wavelet transform and respective mother wavelets are also defined.

3.1 Material, Geometric, and Damage Characteristics of Aluminium Beams

The structures analysed are three aluminium beams with 400 mm length, 40 mm width, and 2.85 mm thickness. The first beam (B1) is undamaged, i.e., the cross-sections have a constant area of 40×2.85 mm^2, whereas the second (B2) and third (B3) beams have two slots created by a milling machine. Table 1 lists the location, depth, width, and thickness reduction of each slot, which can be observed in Fig. 1.

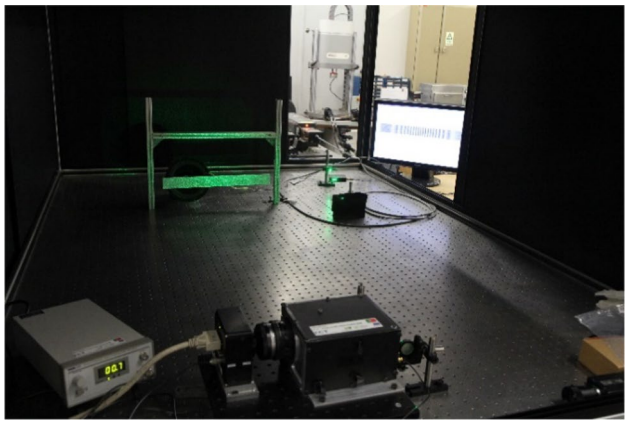

Fig. 2 Experimental set-up for the measurement of modal rotations

3.2 Experimental Set-up for the Measurement of Modal Rotations

The measurement of modal rotations of the three beams is performed by shearography. Shearography is a non-contact, full-field, and high-resolution optical method based on the speckle phenomenon (dos Santos and Lopes 2018). The first step to obtaining the modal rotations is the measurement of natural frequencies by exciting the beams with an impact hammer and acquiring the response with a microphone. The use of the impact hammer and the microphone has the advantage of not adding mass to the beams, which is the case when one uses force transducers and accelerometers. After the input and output signals are sampled, Frequency Response Functions (FRFs) are evaluated. Finally, the natural frequencies are identified from these FRFs by peak analysis.

The experimental set-up for the measurement of the modal rotations of the beams is shown in Fig. 2. In this figure, we can see the speckle effect on the surface of the beam, which is produced by the laser light reflection on the surface. The beams were connected to a frame by two flexible wires glued to each one of the extremities. The damaged beams were placed such that the two slots are facing the opposite side of the inspection surface. To avoid rigid body motions and stabilize the beams, soft foams were placed on the opposite side of the measurement surfaces. The excitation of the beams is accomplished by two loudspeakers,

which are placed close to the surfaces. The laser used to illuminate the beams has 1.3 W of power with a wavelength of 532 nm. To spread the well-collimated light source and obtain a homogeneous illumination, the laser passes through a calibrated lens. An in-house built shearography system using a 4-megapixel camera, Dalsa-Falcon 4M30, was used to record the intensity of the interference pattern produced. This image has a spatial resolution of 2300 pixels in the horizontal direction and 225 pixels in the vertical direction, yielding a sampling interval of 0.17 mm. The high spatial resolution of the measurement makes it possible to describe the modal rotation field with greater precision.

The shearography system uses stroboscopic laser illumination and a temporal phase modulation technique (dos Santos and Lopes 2012). To freeze the speckle pattern, the stroboscopic laser illumination, produced by an acoustic-optic modulation, and the loudspeaker excitation of the beams are synchronized, thus allowing the measurement of the light phase distributions before and after the acoustic excitation and subsequent the light phase change, i.e., the phase map, by phase subtraction. This phase map is afterward filtered and unwrapped by applying the sine/cosine average filter (Aebischer and Waldner 1999) and the Goldstein unwrapping method (Ghiglia and Pritt 1998), respectively. In the present work, the two-dimensional modal rotations $\theta_i(x,y)$ are reduced to one-dimensional profiles $\theta_i(x)$, by considering only the measurement at a line with an y coordinate equal to half the width of the beam. The modal curvatures $\kappa_i(x)$ are computed by applying a combined smoothing and differentiation process (Lopes et al. 2007), leading to a less noisy signal, which is the case if we use finite differences to approximate the derivative of the modal rotations (dos Santos and Lopes 2018). Therefore, the phase map of the i-th mode $\Delta\phi_i(x,y)$ thus obtained is related to the i-th mode first derivative of the out-of-plane displacement, i.e., the rotation $\theta_i(x,y) = \partial w_i(x,y)/\partial x$ by:

$$\Delta\phi_i(x,y) = \frac{4\pi\Delta x}{\lambda}\theta_i(x,y) \tag{1}$$

where λ is the wavelength of the laser (532 nm) and Δx is the shearing amount (5 mm). A more comprehensive description of this type of set-ups and post-processing of captured images for measurement of modal rotations can be found in dos Santos and Lopes (2018) and Francis et al. (2010).

3.3 Evaluation of Changes in Natural Frequencies and Modal Rotations

The changes in the natural frequencies are evaluated by computing the relative percentage difference (RPD) between the i-th natural frequencies of the undamaged beam (B1), f_i, and the two damaged beams (B2 and B3), $\widetilde{f}_i$:

$$RPD(f_i,\widetilde{f}_i) = \left|\frac{f_i - \widetilde{f}_i}{f_i}\right| \times 100 \tag{2}$$

It should be mentioned that in this study, the bold marks were designated to vectors as the ordinary parameters are single arrays and parameters. On this basis, the Modal Assurance Criterion (MAC) (Maia and Silva 1997) between the vectors of the undamaged modal rotations $\boldsymbol{\theta}_i$ and the damaged modal rotations $\widetilde{\boldsymbol{\theta}}_i$ is defined as:

$$MAC\left(\boldsymbol{\theta}_i,\widetilde{\boldsymbol{\theta}}_i\right) = \frac{\left|\boldsymbol{\theta}_i^{\mathrm{T}}\widetilde{\boldsymbol{\theta}}_i\right|^2}{\left|\boldsymbol{\theta}_i^{\mathrm{T}}\boldsymbol{\theta}_i\right|\left|\widetilde{\boldsymbol{\theta}}_i^{\mathrm{T}}\widetilde{\boldsymbol{\theta}}_i\right|} \text{ with } 0 < MAC\left(\boldsymbol{\theta}_i,\widetilde{\boldsymbol{\theta}}_i\right) \le 1 \tag{3}$$

However, the $MAC\left(\boldsymbol{\theta}_i,\widetilde{\boldsymbol{\theta}}_i\right)$ has values that do not differ very much from damage case to damage case. A more sensitive parameter to the changes in modes is the Normalized Modal Difference (NMD) (Maia and Silva 1997; dos Santos et al. 2006):

$$NMD\left(\boldsymbol{\theta}_i,\widetilde{\boldsymbol{\theta}}_i\right) = \sqrt{\frac{1 - MAC\left(\boldsymbol{\theta}_i,\widetilde{\boldsymbol{\theta}}_i\right)}{MAC\left(\boldsymbol{\theta}_i,\widetilde{\boldsymbol{\theta}}_i\right)}} \text{ with } 0 < NMD\left(\boldsymbol{\theta}_i,\widetilde{\boldsymbol{\theta}}_i\right) < \infty \tag{4}$$

Since the RPD is a global parameter, which is related to natural frequencies, whereas the NMD is related to modal characteristics and thus can be seen as a parameter describing local changes, a way to describe both the global and local changes (GLC) due to damage can be defined by:

$$GLC\left((f_i,\widetilde{f}_i,\boldsymbol{\theta}_i,\widetilde{\boldsymbol{\theta}}_i)\right) = RPD(f_i,\widetilde{f}_i) \times NMD\left(\boldsymbol{\theta}_i,\widetilde{\boldsymbol{\theta}}_i\right) \tag{5}$$

3.4 Damage Indicators and Mother Wavelets

The proposed damage identification process requires the measurement of modal rotations of an undamaged beam (B1), to be used as reference data, and the equivalent modal rotations of the two damaged beams (B2 and B3). This leads to the definition of damage indicators based on differences

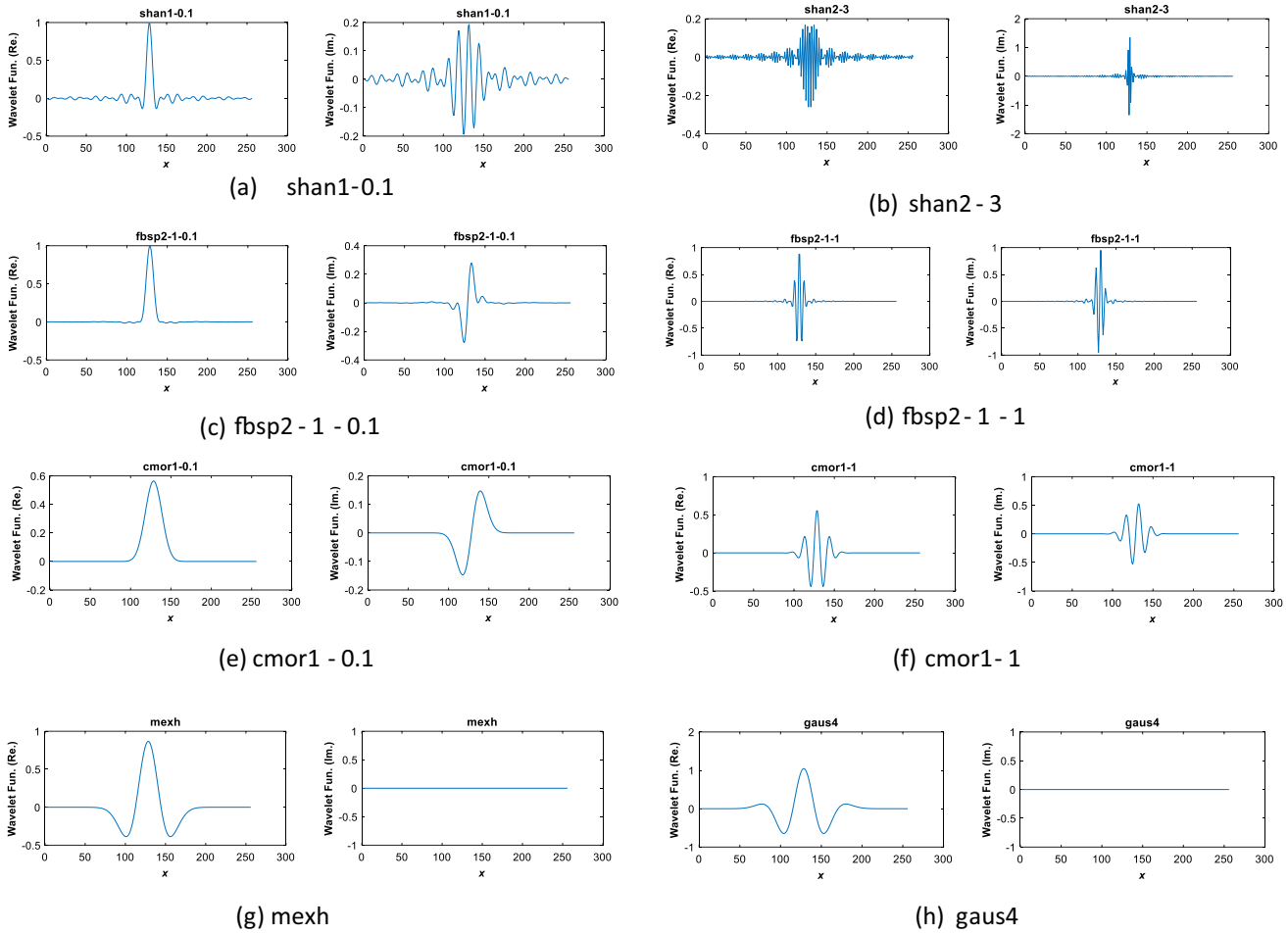

Fig. 3 Plots of some mother wavelets and respective scaling functions

Table 2 Measured natural frequencies of beams 1, 2, and 3 (B1, B2, and B3), RPD and NMD of B2 and B3

Mode	B1	B2			B3		
	Natural frequency [Hz]	Natural frequency [Hz]	RPD [%]	NMD [%]	Natural frequency [Hz]	RPD [%]	NMD [%]
1	92.00	91.25	0.82	0.73	87.00	5.43	4.11
2	254.25	253.00	0.49	1.31	248.50	2.26	8.22
3	499.50	493.00	1.30	2.14	465.00	6.91	11.77

in modal rotations and differences in modal curvatures of the undamaged and damaged beams. A wavelet transform WT, using distinct mother wavelets, is applied to these differences, such that

$$\boldsymbol{MR\&DU}(i) = WT\left(\widetilde{\boldsymbol{\theta}}_i - \boldsymbol{\theta}_i\right) \tag{6}$$

$$\boldsymbol{MC\&DU}(i) = WT\left(\widetilde{\boldsymbol{\kappa}}_i - \boldsymbol{\kappa}_i\right) \tag{7}$$

for the damage indicators based on modal rotations $\boldsymbol{MR\&DU}(i)$ and modal curvatures $\boldsymbol{MC\&DU}(i)$, respectively, of the i-th mode.

Time–frequency analysis has been mentioned in different historical contexts. In 1807, Joseph Fourier proposed that every static function could be represented as an infinite number of sine waves and cosine waves of different frequencies (Hanteh et al. 2021). The proposed transform, nowadays called the Fourier transform, was the first to transfer time domain information to the frequency domain

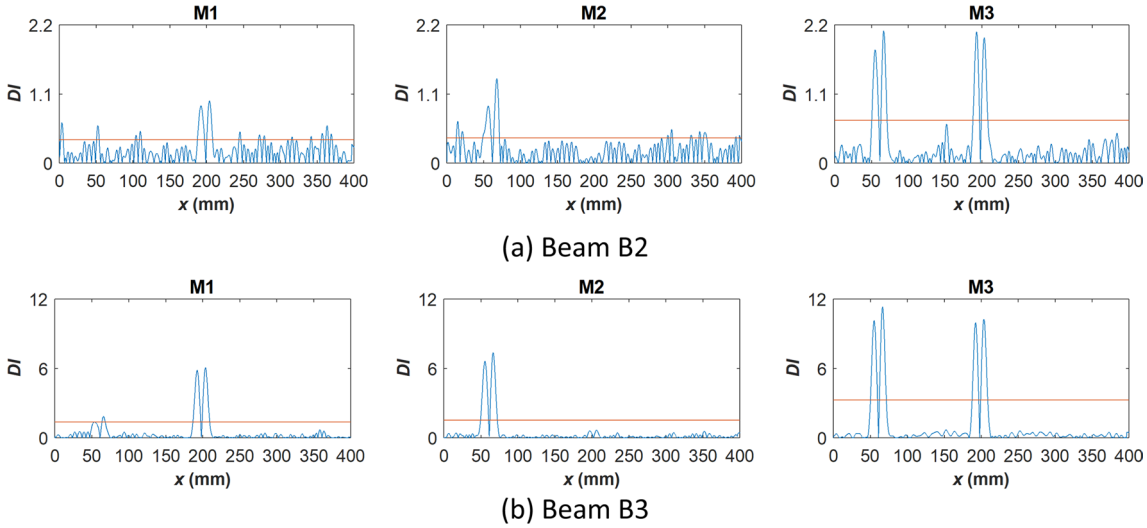

Fig. 4 Absolute values of wavelet coefficients with *shan1-0.1* wavelet applied to modal curvatures M1, M2, and M3

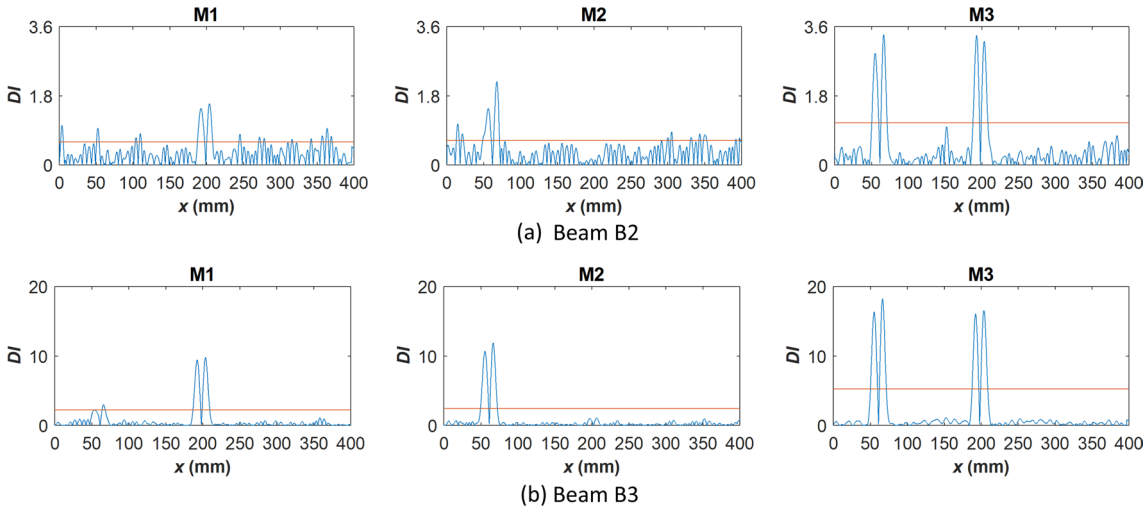

Fig. 5 Absolute values of wavelet coefficients with *fbsp2-1-0.1* wavelet applied to modal curvatures M1, M2, and M3

and find out the prominent frequencies in the signal. This idea was expanded to non-static functions with a changing statistical distribution over time. It was gradually understood that information could be centred on time and frequency when signals are broken up into separate components that are not pure sine waves. There are various families that can generate and modify signals over both time and frequency domains, such that any signal can be converted into a set of local basic functions, also called mother wavelets (Hanteh and Rezaifar 2021). An example of a wavelet transform application would be an analysis that shows how the frequencies change within a short time period. Basically, this transform produces the frequency components for different resolutions by varying the mother wavelets. These mother wavelets can be used to analyse each local property of a signal (Jahangir and Esfahani 2013). Wavelet transforms are sensitive to singularities in signals, and thus they are often able to detect abrupt changes in mode shapes due to the presence of damage.

In the present work, the post-processing of differences in modal rotations and differences in modal curvatures is carried out by applying a continuous wavelet analysis, which is defined below. A signal $x(t) \in [-\infty, +\infty]$ can be analysed by 1D continuous wavelet according to:

$$CWT(s,b) = \frac{1}{\sqrt{|s|}} \int_{-\infty}^{+\infty} x(t) \Psi^* \left(\frac{t-b}{s} \right) dt \tag{8}$$

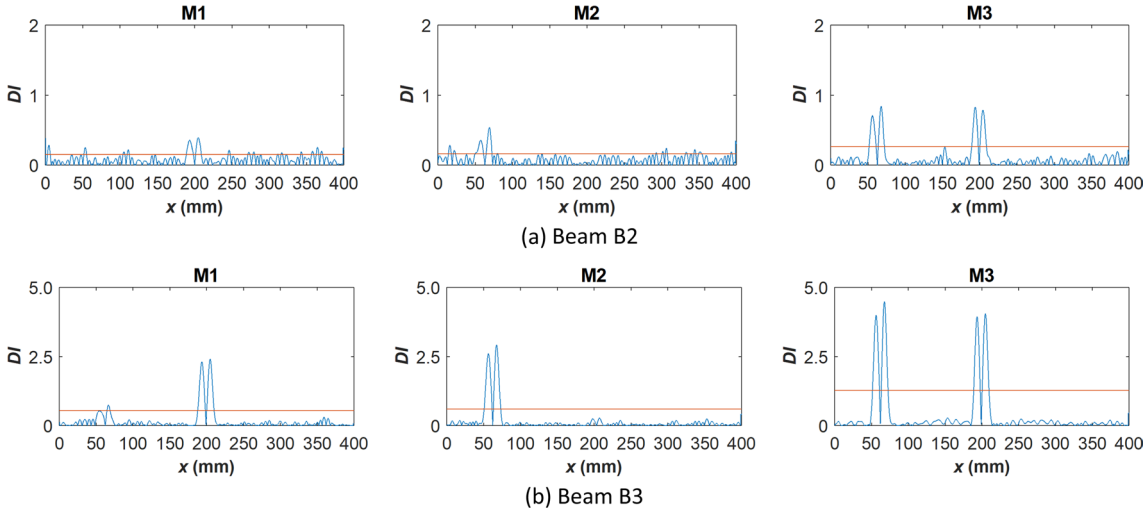

Fig. 6 Absolute values of wavelet coefficients with *cmor1-0.1* wavelet applied to modal curvatures M1, M2, and M3

Table 3 Total number of identified slots by each family and average number of slots identified by one wavelet of a given family

Wavelet family	Number of mother wavelets in the family	Total no. of identified slots	Average no. of identified slots by one wavelet
Daubechies	10	12	1.2000
Symlets	7	6	0.8571
Coiflets	5	0	0.0000
Biorthogonal	15	28	1.7333
Reverse biorthogonal	15	32	2.1333
Meyer	1	0	0.0000
Discrete approximation of Meyer	1	0	0.0000
Gaussian	8	6	0.7500
Mexican hat	1	0	0.0000
Morlet	1	0	0.0000
Complex Gaussian	5	4	0.8000
Shannon	5	33	6.6000
Frequency B-Spline	6	30	5.0000
Complex Morlet	4	18	4.5000

Table 4 Values of GLC and total number of identified slots in B2 and B3 by all mother wavelets

Mode	B2				B3			
	GLC	S1	S2	S1 + S2	GLC	S1	S2	S1 + S2
1	0.5939	6	0	6	22.3373	33	5	38
2	0.6420	1	5	6	18.5932	0	31	31
3	2.7850	21	22	43	81.3145	9	34	43

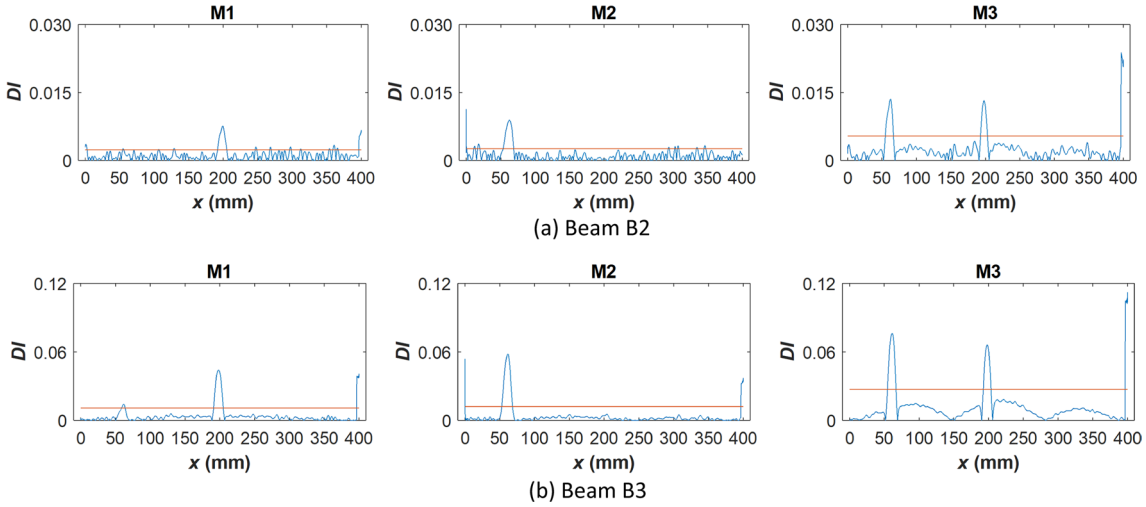

Fig. 7 Absolute values of wavelet coefficients with *shan1-0.1* wavelet applied to modal rotations M1, M2, and M3

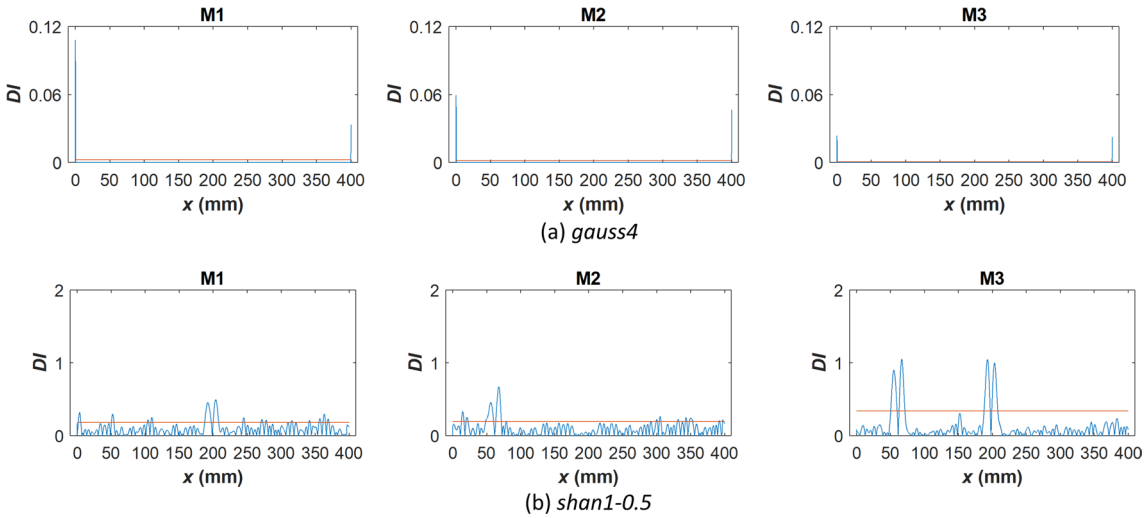

Fig. 8 Absolute values of wavelet coefficients with, **a** *gaus4* and **b** *shan1-0.5* wavelets applied to modal curvatures M1, M2, and M3 of beam B2

The translation and scaling parameters are b and s, t is the time change defined for each mother wavelet function and $CWT(s,b)$ are the wavelet coefficients. $\Psi^*(s,b,t)$ is the mother wavelet, being its complex conjugate given by:

$$\Psi^*(s,b,t) = \frac{1}{\sqrt{|s|}}\Psi\left(\frac{t-b}{s}\right) \tag{9}$$

The differences in modal rotations and the differences in modal curvatures were post-processed, according to Eqs. (6) and (7), respectively, with 14 distinct wavelet families and a total of 84 mother wavelets. The families and respective mother wavelets are described in Matlab software (2014). Some of the mother wavelets are depicted in Fig. 3.

4 Results and Discussion

This section contains a preliminary analysis of the differences in natural frequencies and the changes in modal rotations. Damage identifications obtained by post-processing differences in modal curvatures and modal rotations are also presented and discussed. In view of the results, the adequacy and ability of each mother wavelet, each wavelet family, and each mode to successfully identify the damage is verified. Finally, a study on the boundary effect and noise on the identifications as a function of the mother wavelet applied is also presented.

4.1 Differences in Natural Frequencies and Changes in Modal Rotations

Table 2 lists the natural frequencies of the three beams, the relative percentage difference (RPD) between the natural frequencies of the undamaged beam B1 and the damaged beams B2 and B3, and the normalized modal difference (NMD) of the modal rotations. It can be seen that beam B2 has lower values of these parameters than beam B3, thus indicating that the reduction in thickness at the slots of beam B2 is smaller than the one of beam B3.

4.2 Damage Identification Results

4.2.1 Wavelet Families, Mother Wavelets, Modes, and Modal Characteristic

The ability of the distinct mother wavelets to identify both slots in beams B2 and B3 with the post-processing of differences in modal curvatures, as defined by Eq. (7), can be seen in Table 5 of Appendix A, where the peak values (PV) of the wavelet coefficients in both slots of the two beams are listed as a function of the wavelet mothers and modes. This Table is the result of an automated procedure that looks for the two highest PV and verifies if they are located at the positions of the slots. If not, the identification of a slot is taken as unsuccessful, and an em dash is assigned to it. It is clear that Shannon, frequency B-spline, and complex Morlet wavelets are more efficient in identifying the slots. Indeed, as reported in Figs. 4, 5, and 6, the PV of wavelet coefficients for *shan1-0.1*, *fbsp2-1-0.1,* and *cmor1-0.1* are located at the site of the slots and have larger values than the ones given by other families, and no boundary effect is observed. It is worth noting that with the same wavelet and mode, the PV is higher in beam B3 than in beam B2. For example, with the *shan1-0.1* wavelet and mode M3 we obtain a maximum of 2.1040 in beam B2 for slot 2 and 11.317 for this same slot.

In this paper, 14 wavelet families including 84 mother wavelets were considered to detect the location of single and double slots in the tested aluminium beams. After applying each wavelet family and the predefined damage thresholds, the number of times that wavelet family was successful in identifying the exact location of the slot (s) was counted to determine the best wavelet family among others. Table 3 lists the total number of identified slots by applying all the mother wavelets within each family and the average number of slots identified by one wavelet of a given family. This average is evaluated by computing the ratio of the total number of identified slots within each family to the total number of mother wavelets in the family, which is presented in the second column of Table 3. It can be seen that the Shannon and frequency B-spline families are the ones with the largest average number of identified slots by one wavelet, followed by the complex Morlet family. Although the total number of identified slots with the biorthogonal and reverse biorthogonal families is high, i.e., 32 and 28, respectively, the average number of identified slots is around two since 15 mother wavelets were tested for each one of these families.

It is also noteworthy that with mode M3 both slots are identified, and the absolute values of the wavelet coefficients are high and approximately the same. In Table 4 we can see the values of the GLC parameter for the three modes and notice the large values of this parameter for mode M3, which indicates that the most changed mode is the third and, thus, more sensitive to damage. Indeed, in beam B2 we have a GLC of mode M3, which is one order of magnitude larger

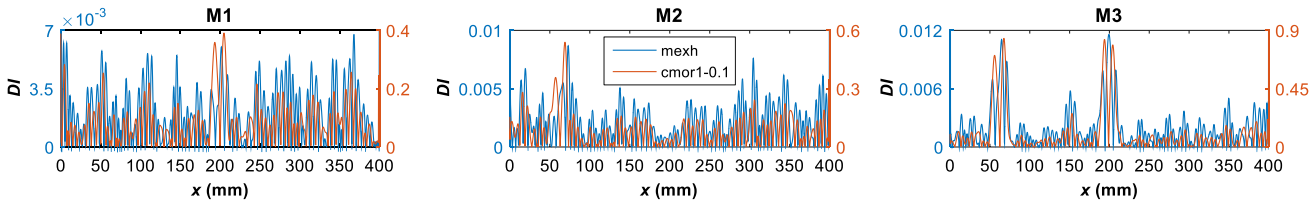

Fig. 9 Absolute values of wavelet coefficients with *mexh* and *cmor1-0.1* wavelets applied to modal curvatures M1, M2, and M3 of beam B2

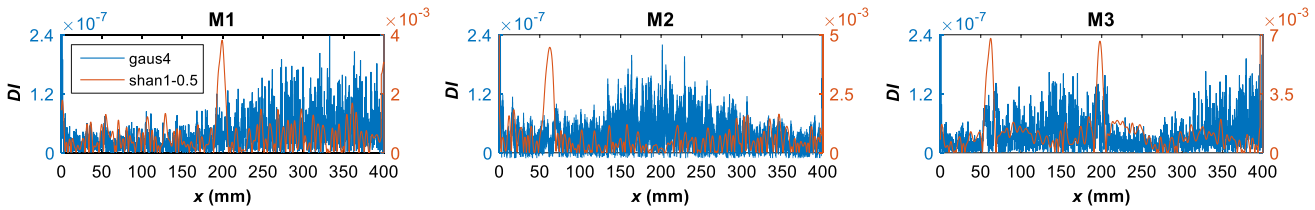

Fig. 10 Absolute values of wavelet coefficients with *gaus4* and *shan1-0.5* wavelets applied to modal rotations M1, M2, and M3 of beam B2

than the GLC of the other two modes, and the number of identified slots is 43 with M3 and 6 for modes M1 and M2, thus indicating a good correlation between GLC of a mode and its ability to identify damage.

Another modal characteristic that can be post-processed besides the modal curvature is modal rotation. However, the post-processing of difference in modal rotations, based on Eq. (6), with *shan1-0.1* and *fbsp2-1–0.1* and *cmor1-0.1* yields less satisfactory identifications of the slots than the post-processing of differences in modal curvatures, since, as seen in Fig. 7, the results exhibit boundary effects. We can also observe in Fig. 7 that for mode M3 the results show humps. It is thus advisable to read the results obtained with modal rotations data with care and as a complement to the ones given by post-processing the differences in modal curvatures.

4.2.2 Boundary Effect and Noise

A problem often found in the analysis of signals with wavelets, in particular in the application of wavelet transform to damage identification, is the existence of boundary effects in the results. Another issue is that some wavelets yield very noisy results, such that the noise masks the damage influence, and no clear peak at the damage locations can be observed. The existence of these undesirable characteristics is more noticeable when one tries to identify small damage and thus, only results with beam B2 are reported here.

The picking up of the wavelets with results where the boundary effect is more and less noticeable is carried out by evaluating the ratio of the maximum value at the left and right extremities to the maximum value in the other zones of the beam. The mother wavelet where we observe the largest boundary effect in the results is *gauss4*, as reported in Fig. 8a. It is perfectly clear that with this wavelet we are not able to identify the slots. Figure 8b presents the results with the *shan1-0.5*, which is the wavelet where we have no boundary effect, and thus it is possible to unmistakably localize the slots.

The mother wavelets with more and less noisy results were found by counting the number of fluctuations (peaks) that surpassed the threshold value (Sarmadi et al. 2021). In this search, the values of the coefficients in the extremities were not taken into account. For the modal curvature post-processing, the noisiest results are obtained with the *coif4*, *mexh* and *cgau4* mother wavelets, whereas the *sym6* and *cmor1-0.1* mother wavelets yield less noisy identifications. It should be mentioned that the sensitivity of mother wavelets and the influence of noise can be related directly to their mathematical properties as the noisiest mother wavelets such as *coif4*, *mexh* and *cgau4* mother wavelets resulted in more noisy coefficients and smoothest mother wavelets such as *sym6* and *cmor1-0.1* mother wavelets resulted in less noisy detections. Figure 9 shows the results of the application of *mexh* and *cmor1-0.1* wavelets to modal curvatures. We can observe that the *mexh* wavelet does not allow the correct identification of the slots. The results with the post-processing of modal rotations with *gaus4* present the highest level of noise, whereas the *shan1-0.5* (*fbsp1-1-0.5*), *shan1-0.1* and *fbsp2-1-0.1* mother wavelets give the least noisy identifications. Indeed, as can be observed in Fig. 10, contrary to the *shan1-0.5* wavelet, which has clear peaks at the positions of the slots, the *gaus4* mother wavelet yields only noise, making it impossible to locate the slots.

5 Conclusions

The selection of the best mother wavelets and mode for successful multiple damage identification in aluminium beams is reported in this paper. The modal rotations are experimentally measured with shearography. The differences in modal rotations and differences in modal curvatures are post-processed by continuous wavelet transform with 14 wavelet families and 84 mother wavelets. A novel parameter for the selection of the best mode, based on the measurement of global and local modal changes due to damage, is proved to be effective.

In general, families with complex mother wavelets yield the best damage identification results, namely the Shannon, frequency B-spline, and complex Morlet families, since the average number of identified slots by each wavelet belonging to these families is the highest. Furthermore, this type of wavelets, contrary to Gaussian wavelets, present the lowest noise in the results and are not sensitive to boundary effects. Among the mother wavelets belonging to the aforementioned families, the highest values of the absolute values of coefficients of *shan1-0.1*, *fbsp2-1–0.1,* and *cmor1-0.1* mother wavelets are observed at the slot locations. It is noteworthy that these three wavelets have the same bandwidth parameter and centre frequency, 1 and 0.1, respectively. In brief, the reported damage identification results clearly show that the combination of shearography measurements and a proper selection of mother wavelets can lead to successful multiple damage identifications in beams. This success can be further improved by selecting the most changed mode according to the proposed selection parameter.

Appendix A

Table 5 lists the peak values (PV) of wavelet coefficients in both slots of the two beams as a function of the first three modal curvatures, according to Eq. (7). The identifications of the peaks are made automatically by looking for the maximum of the wavelet coefficients.

Table 5 Peak values (PV) of wavelet coefficients in slots S1 and S2 of beams B2 and B3 for modal curvatures M1, M2, and M3

Wavelet	B2						B3					
	M1		M2		M3		M1		M2		M3	
	S1	S2	S1	S2	S1	S2	S1	S2	S1	S2	S1	S2
Daubechies												
db1 = haar	–	–	–	–	–	–	–	–	–	–	–	–
db2	–	–	–	–	–	–	–	–	–	–	–	–
db3	–	–	–	–	–	–	–	–	–	–	–	–
db4	–	–	–	–	–	–	0.0510	–	–	–	–	–
db5	–	–	–	–	–	–	0.0720	–	–	0.0870	–	0.1340
db6	–	–	–	–	–	–	0.0550	–	–	0.0670	–	0.1030
db7	–	–	–	–	–	–	–	–	–	–	–	–
db8	–	–	–	–	–	–	0.0380	–	–	–	–	–
db9	–	–	–	–	–	–	0.0680	–	–	–	–	0.1270
db10	–	–	–	–	–	–	–	–	–	0.0380	–	0.0580
Symlets												
sym2	–	–	–	–	–	–	–	–	–	0.0640	–	0.0980
sym3	–	–	–	–	–	–	–	–	–	–	–	–
sym4	–	–	–	–	–	–	–	–	–	–	–	–
sym5	–	–	–	–	–	–	–	–	–	0.0660	–	0.1020
sym6	–	–	–	–	–	–	–	–	–	–	–	–
sym7	–	–	–	–	–	–	0.0590	–	–	–	–	0.1100
sym8	–	–	–	–	–	–	–	–	–	–	–	–
Coiflets												
coif1	–	–	–	–	–	–	–	–	–	–	–	–
coif2	–	–	–	–	–	–	–	–	–	–	–	–
coif3	–	–	–	–	–	–	–	–	–	–	–	–
coif4	–	–	–	–	–	–	–	–	–	–	–	–
coif5	–	–	–	–	–	–	–	–	–	–	–	–
Wavelet	B2						B3					
	M1		M2		M3		M1		M2		M3	
	S1	S2	S1	S2	S1	S2	S1	S2	S1	S2	S1	S2
Biorthogonal												
bior1.1	–	–	–	–	–	–	–	–	–	–	–	–
bior1.3	–	–	–	–	–	–	–	–	–	–	–	–
bior1.5	–	–	–	–	–	–	–	–	–	–	–	–
bior2.2	–	–	–	–	–	–	–	–	–	–	–	–
bior2.4	–	–	–	–	–	–	–	–	–	–	–	–
bior2.6	–	–	–	–	–	–	–	–	–	–	–	–
bior2.8	–	–	–	–	–	–	–	–	–	–	–	–
bior3.1	–	–	–	–	0.2168	0.2200	0.6300	–	–	0.7660	1.0600	1.1760
bior3.3	–	–	–	–	0.0926	0.0940	0.2680	–	–	0.3260	–	0.5000
bior3.5	–	–	–	–	0.0756	0.0770	0.2190	–	–	0.2660	–	0.4080
bior3.7	–	–	–	–	0.0705	0.0710	0.2040	–	–	0.2480	–	0.3810
bior3.9	–	–	–	–	0.0683	0.0690	0.1980	–	–	0.2410	–	0.3700
bior4.4	–	–	–	–	–	–	–	–	–	–	–	–
bior5.5	–	–	–	–	–	–	–	–	–	–	–	–
bior6.8	–	–	–	–	–	–	–	–	–	–	–	–
Reverse biorthogonal												
rbio1.1	–	–	–	–	–	–	0.0000	–	–	–	–	0.0000

Table 5 (continued)

Wavelet	B2						B3					
	M1		M2		M3		M1		M2		M3	
	S1	S2	S1	S2	S1	S2	S1	S2	S1	S2	S1	S2
rbio1.3	–	–	–	–	0.0270	0.0270	0.0780	–	–	0.0950	–	0.1460
rbio1.5	–	–	–	–	0.0268	0.0270	0.0780	–	–	0.0940	–	0.1450
rbio2.2	–	–	–	–	–	–	–	–	–	–	–	–
rbio2.4	–	–	–	–	–	–	–	–	–	–	–	–
rbio2.6	–	–	–	–	–	–	–	–	–	–	–	–
rbio2.8	–	–	–	–	–	–	–	–	–	–	–	–
rbio3.1	–	–	–	–	0.0726	0.0730	0.2100	–	–	0.2550	0.3532	0.3920
rbio3.3	–	–	–	–	–	–	0.0260	–	–	0.0320	–	0.0490
rbio3.5	–	–	–	–	0.0091	0.0090	0.0260	–	–	0.0320	–	0.0490
rbio3.7	–	–	–	–	–	–	0.0260	–	–	0.0320	–	0.0490
rbio3.9	–	–	–	–	–	–	0.0260	–	–	0.0320	–	0.0490
rbio4.4	–	–	–	–	–	–	–	–	–	–	–	–
rbio5.5	–	–	–	–	–	–	–	–	–	–	–	–
rbio6.8	–	–	–	–	–	–	–	–	–	–	–	–
Wavelet	B2						B3					
	M1		M2		M3		M1		M2		M3	
	S1	S2	S1	S2	S1	S2	S1	S2	S1	S2	S1	S2
Meyer												
meyr	–	–	–	–	–	–	–	–	–	–	–	–
Disc. Meyer												
dmey	–	–	–	–	–	–	–	–	–	–	–	–
Gaussian												
gaus1	–	–	–	–	0.1727	0.1750	0.5000	–	–	0.6070	0.8409	0.9320
gaus2	–	–	–	–	–	–	–	–	–	–	–	–
gaus3	–	–	–	–	–	–	–	–	–	–	–	–
gaus4	–	–	–	–	–	–	–	–	–	–	–	–
gaus5	–	–	–	–	–	–	–	–	–	–	–	–
gaus6	–	–	–	–	–	–	–	–	–	–	–	–
gaus7	–	–	–	–	–	–	–	–	–	–	–	–
gaus8	–	–	–	–	–	–	–	–	–	–	–	–
Mexican hat												
mexh	–	–	–	–	–	–	–	–	–	–	–	–
Morlet												
morl	–	–	–	–	–	–	–	–	–	–	–	–
Complex Gaussian												
cgau1	–	–	–	–	–	–	0.2760	–	–	0.3350	0.4642	0.5150
cgau2	–	–	–	–	–	–	–	–	–	–	–	–
cgau3	–	–	–	–	–	–	–	–	–	–	–	–
cgau4	–	–	–	–	–	–	–	–	–	–	–	–
cgau5	–	–	–	–	–	–	–	–	–	–	–	–
Wavelet	M1		M2		M3		M1		M2		M3	
	S1	S2	S1	S2	S1	S2	S1	S2	S1	S2	S1	S2
Shannon												
shan1-1.5	–	–	–	–	0.0034	0.0036	0.0100	–	–	0.0130	–	0.0190
shan1-1	–	–	–	–	0.0061	0.0060	0.0180	–	–	0.0220	–	0.0330

Table 5 (continued)

Wavelet	M1		M2		M3		M1		M2		M3	
	S1	S2	S1	S2	S1	S2	S1	S2	S1	S2	S1	S2
shan1-0.5	0.4958	–	–	0.6743	1.0470	1.0530	3.0400	0.9259	–	3.6910	5.1370	5.6670
shan1-0.1	0.9908	–	–	1.3470	2.0910	2.1040	6.0700	1.8520	–	7.3740	10.260	11.317
shan2-3	–	–	–	–	0.0013	0.0012	0.0040	–	–	0.0050	–	0.0070
Frequency B-Spline												
fbsp1-1–1.5	–	–	–	–	0.0034	0.0036	0.0100	–	–	0.0130	–	0.0190
fbsp1-1–1	–	–	–	–	0.0060	0.0061	0.0180	–	–	0.0220	–	0.0330
fbsp1-1–0.5	0.4960	–	0.4960	–	1.0470	1.0530	3.0400	–	–	3.6910	–	5.6670
fbsp2-1–1	–	–	–	–	–	–	–	–	–	–	–	–
fbsp2-1–0.5	–	–	–		–	0.0290	0.0820	–	–	0.1010	–	0.1530
fbsp2-1–0.1	1.5960	–	–	2.1720	3.3730	3.3910	9.7890	2.9840	–	11.889	16.540	18.250
Complex Morlet												
cmor1-1.5	–	–	–	–	–	–	–	–	–	–	–	–
cmor1-1	–	–	–	–	–	–	–	–	–	–	–	–
cmor1-0.5	0.0370	–	–	0.0506	0.0778	0.0790	0.2250	0.0698	–	0.2740	0.3793	0.4200
cmor1-0.1	0.3910	–	–	0.5391	0.8300	0.8390	2.4040	0.7441	–	2.9210	4.0470	4.4840

Acknowledgements The first author and third author would like to acknowledge the support of FCT, through IDMEC, under LAETA, project UIDB/50022/2020.

Funding No funding was received for conducting this study.

Declarations

Conflict of interest The authors have no relevant financial or non-financial interests to disclose.

References

Abdel-Latif AM (2009) An overview of the applications of NDI/NDT in engineering design for structural integrity and damage tolerance in aircraft structures. Damage Fract Mech Fail Anal Eng Mater Struct. https://doi.org/10.1007/978-90-481-2669-9_10

Abdulkareem M, Bakhary N, Vafaei M et al (2019) Application of two-dimensional wavelet transform to detect damage in steel plate structures. Meas J Int Meas Confed 146:912–923. https://doi.org/10.1016/j.measurement.2019.07.027

Abry P (1997) Ondelettes et turbulence. Multirésolutions, algorithmes de décomposition, invariance d'échelles. Diderot multimédia, Paris

Aebischer HA, Waldner S (1999) A simple and effective method for filtering speckle-interferometric phase fringe patterns. Opt Commun 162:205–210. https://doi.org/10.1016/S0030-4018(99)00116-9

Araujo Dos Santos JV, Katunin A, Lopes H (2019) Vibration-based damage identification using wavelet transform and a numerical model of shearography. Int J Struct Stab Dyn 19:1–28. https://doi.org/10.1142/S021945541950038X

Bagheri M, Chahkandi A, Jahangir H (2019) Seismic reliability analysis of RC frames rehabilitated by glass fiber-reinforced polymers. Int J Civ Eng. https://doi.org/10.1007/s40999-019-00438-x

Daubechies I (1992) Ten lectures on wavelets. SIAM, Philadelphia, PA

dos Santos JVA, Lopes H (2018) Damage localization based on modal response measured with shearography. In: Nobari AS, Aliabadi FMH (eds) Vibration-based techniques for damage detection and localization in engineering structures. World Scientific Publishing, New Jersey, pp 141–172

dos Santos JVA, Lopes HMR, Vaz M et al (2006) Damage localization in laminated composite plates using mode shapes measured by pulsed TV holography. Compos Struct 76:272–281. https://doi.org/10.1016/j.compstruct.2006.06.034

dos Santos JVA, Lopes H, Katunin A (2021) Damage identification in beams by post-processing modal displacements and rotations with haar wavelet. In: Rizzo P, Milazzo A (eds) European workshop on structural health monitoring. Springer International Publishing, Cham, pp 817–824

Douka E, Loutridis S, Trochidis A (2003) Crack identification in beams using wavelet analysis. Int J Solids Struct 40:3557–3569. https://doi.org/10.1016/S0020-7683(03)00147-1

Douka E, Loutridis S, Trochidis A (2004) Crack identification in plates using wavelet analysis. J Sound Vib 270:279–295. https://doi.org/10.1016/S0022-460X(03)00536-4

Fan W, Qiao P (2009) A 2-D continuous wavelet transform of mode shape data for damage detection of plate structures. Int J Solids Struct 46:4379–4395. https://doi.org/10.1016/j.ijsolstr.2009.08.022

Feng D, Feng MQ (2018) Computer vision for SHM of civil infrastructure: from dynamic response measurement to damage detection—a review. Eng Struct 156:105–117. https://doi.org/10.1016/j.engstruct.2017.11.018

Francis D, Tatam RP, Groves RM (2010) Shearography technology and applications: a review. Meas Sci Technol 21:102001. https://doi.org/10.1088/0957-0233/21/10/102001

Gentile A, Messina A (2003) On the continuous wavelet transforms applied to discrete vibrational data for detecting open cracks in damaged beams. Int J Solids Struct 40:295–315. https://doi.org/10.1016/S0020-7683(02)00548-6

Ghiglia DC, Pritt MD (1998) Two-dimensional phase unwrapping: theory, algorithms, and software. Wiley-Interscience, New York

Grandt F (2011) Damage tolerant design and nondestructive inspection—keys to aircraft airworthiness. Procedia Eng 17:236–246. https://doi.org/10.1016/j.proeng.2011.10.025

Hanteh M, Rezaifar O (2021) Damage detection in precast full panel building by continuous wavelet analysis analytical method. Structures 29:701–713. https://doi.org/10.1016/j.istruc.2020.12.002

Hanteh M, Rezaifar O, Gholhaki M (2021) Selecting the appropriate wavelet function in the damage detection of precast full panel building based on experimental results and wavelet analysis. J Civ Struct Heal Monit 11:1013–1036. https://doi.org/10.1007/s13349-021-00497-6

Huang Y, Meyer D, Nemat-Nasser S (2009) Damage detection with spatially distributed 2D continuous wavelet transform. Mech Mater 41:1096–1107. https://doi.org/10.1016/j.mechmat.2009.05.006

Jahangir H, Esfahani MR (2020a) Experimental analysis on tensile strengthening properties of steel and glass fiber reinforced inorganic matrix composites. Sci Iranica 4:7. https://doi.org/10.24200/SCI.2020.54787.3921

Jahangir H, Esfahani MR (2020b) Investigating loading rate and fibre densities influence on SRG-concrete bond behaviour. Steel Compos Struct 34:877–889. https://doi.org/10.12989/scs.2020.34.6.877

Jahangir H, Bagheri M, Delavari SMJ (2021a) Cyclic behavior assessment of steel bar hysteretic dampers using multiple nonlinear regression approach. Iranian J Sci Technol Trans Civ Eng 45:1227–1251. https://doi.org/10.1007/s40996-020-00497-4

Jahangir H, Khatibinia M, Kavousi M (2021b) Application of contourlet transform in damage localization and severity assessment of prestressed concrete slabs. J Soft Comput Civ Eng 5:39–68. https://doi.org/10.22115/SCCE.2021.282138.1301

Jahangir H, Esfahani MR (2012) Structural damage identification based on modal data and wavelet analysis. In: 3rd National Conference on Earthquake & Structure. Kerman, Iran

Jahangir H, Esfahani MR (2013) Damage localization of structures using adaptive neuro-fuzzy inference system. In: 7th National Congress on Civil Engineering. Zahedan, Iran

Janeliukstis R, Rucevskis S, Wesolowski M, Chate A (2017) Experimental structural damage localization in beam structure using spatial continuous wavelet transform and mode shape curvature methods. Meas J Int Meas Confed 102:253–270. https://doi.org/10.1016/j.measurement.2017.02.005

Katunin A, Holewik F (2013) Crack identification in composite elements with non-linear geometry using spatial wavelet transform. Arch Civ Mech Eng 13:287–296. https://doi.org/10.1016/j.acme.2013.02.003

Katunin A, Lopes H, Dos Santos JVA (2018) Enhancement of shearography-based damage identification using best tree wavelet packet analysis. MATEC Web Conf. https://doi.org/10.1051/matecconf/201820406002

Katunin A, Lopes H, dos Santos JVA (2019) Identification of multiple damage using modal rotation obtained with shearography and undecimated wavelet transform. Mech Syst Signal Process 116:725–740. https://doi.org/10.1016/j.ymssp.2018.07.024

Katunin A, Araújo dos Santos JV, Lopes H (2021) Damage identification by wavelet analysis of modal rotation differences. Structures 30:1–10. https://doi.org/10.1016/j.istruc.2021.01.010

Lopes HMR, Guedes RM, Vaz MA (2007) An improved mixed numerical-experimental method for stress field calculation. Opt Laser Technol 39:1066–1073. https://doi.org/10.1016/j.optlastec.2006.04.006

Lopes H, Ribeiro J, Dos Santos AJV (2012) Interferometric techniques in structural damage identification. Shock Vib 19:835–844. https://doi.org/10.3233/SAV-2012-0692

Lopes H, Ferreira F, Araújo Dos Santos JV, Moreno-García P (2014) Localization of damage with speckle shearography and higher order spatial derivatives. Mech Syst Signal Process 49:24–38. https://doi.org/10.1016/j.ymssp.2013.12.016

Loutridis S, Douka E, Trochidis A (2004) Crack identification in double-cracked beams using wavelet analysis. J Sound Vib 277:1025–1039. https://doi.org/10.1016/j.jsv.2003.09.035

Maia NMM, Silva JMM (1997) Theoretical and experimental modal analysis. Wiley, New York

Mininni M, Gabriele S, Lopes H, Araújo dos Santos JV (2016) Damage identification in beams using speckle shearography and an optimal spatial sampling. Mech Syst Signal Process 79:47–64. https://doi.org/10.1016/j.ymssp.2016.02.039

Misiti M, Misiti Y, Oppenheim G, Poggi JM (2014) Wavelet Toolbox User's Guide, Rev. 4.14. The MathWorks. Inc

Mousavi AA, Zhang C, Masri SF, Gholipour G (2021) Damage detection and localization of a steel truss bridge model subjected to impact and white noise excitations using empirical wavelet transform neural network approach. Measurement 185:110060. https://doi.org/10.1016/j.measurement.2021.110060

Nayyar A, Baneen U, Naqvi SAZ, Ahsan M (2021) Detection and localization of multiple small damages in beam. Adv Mech Eng 13:1687814020987329. https://doi.org/10.1177/1687814020987329

Reis Lopes HM, Araújo Dos Santos JV, Mota Soares CM et al (2011) A numerical-experimental method for damage location based on rotation fields spatial differentiation. Comput Struct 89:1754–1770. https://doi.org/10.1016/j.compstruc.2011.03.014

Rucka M, Wilde K (2006) Application of continuous wavelet transform in vibration based damage detection method for beams and plates. J Sound Vib 297:536–550. https://doi.org/10.1016/j.jsv.2006.04.015

dos Santos JVA, Lopes H (2012) Application of speckle interferometry to damage identification. In: Topping BH V (ed). Saxe-Coburg Publications, Stirlingshire, UK, pp 299--330, in Computational Methods for Engineering

Sarmadi H, Entezami A, Salar M, De Michele C (2021) Bridge health monitoring in environmental variability by new clustering and threshold estimation methods. J Civ Struct Heal Monit 11:629–644. https://doi.org/10.1007/s13349-021-00472-1

Seyedi SR, Keyhani A, Jahangir H (2015) An energy-based damage detection algorithm based on modal data. In: 7th International conference on seismology & earthquake engineering. International Institute of Earthquake Engineering and Seismology (IIEES), pp 335–336

Solís M, Algaba M, Galvín P (2013) Continuous wavelet analysis of mode shapes differences for damage detection. Mech Syst Signal Process 40:645–666. https://doi.org/10.1016/j.ymssp.2013.06.006

Solís M, Ma Q, Galvín P (2018) Damage detection in beams from modal and wavelet analysis using a stationary roving mass and noise estimation. Strain 54:1–18. https://doi.org/10.1111/str.12266

Teolis A (1998) Computational signal processing with wavelets. Birkhäuser Boston, Boston

Yang C, Oyadiji SO (2017) Delamination detection in composite laminate plates using 2D wavelet analysis of modal frequency surface. Comput Struct 179:109–126. https://doi.org/10.1016/j.compstruc.2016.10.019

Yazdanpanah O, Mohebi B, Yakhchalian M (2020) Selection of optimal wavelet-based damage-sensitive feature for seismic damage diagnosis. Measurement 154:107447. https://doi.org/10.1016/j.measurement.2019.107447

Yazdanpanah O, Formisano A, Chang M, Mohebi B (2021) Fragility curves for seismic damage assessment in regular and irregular MRFs using improved wavelet-based damage index. Measurement 182:109558. https://doi.org/10.1016/j.measurement.2021.109558

Zhao Q, Dan X, Sun F et al (2018) Digital shearography for NDT: Phase measurement technique and recent developments. Appl Sci (switzerland). https://doi.org/10.3390/app8122662

Zhou J, Li Z, Chen J (2018) Damage identification method based on continuous wavelet transform and mode shapes for composite laminates with cutouts. Compos Struct 191:12–23. https://doi.org/10.1016/j.compstruct.2018.02.028

Zhu YK, Tian GY, Lu RS, Zhang H (2011) A review of optical NDT technologies. Sensors 11:7773–7798. https://doi.org/10.3390/s110807773